

Contents lists available at ScienceDirect

Surface Science

journal homepage: www.elsevier.com/locate/susc



CO-induced inversion of the layer sequence of a model CoCu catalyst



Greg Collinge ^a, Yizhi Xiang ^a, Roland Barbosa ^a, Jean-Sabin McEwen ^{a,b,c}, Norbert Kruse ^{a,*}

- ^a The Gene & Linda Voiland School of Chemical Engineering and Bioengineering, Washington State University, Pullman, WA 99164, USA
- b Department of Physics and Astronomy, Washington State University, Pullman, WA 99164, USA
- ^c Department of Chemistry, Washington State University, Pullman, WA 99164, USA

ARTICLE INFO

Available online 19 October 2015

Keywords: Bimetallic CoCu CO-induced segregation Fischer–Tropsch CO adsorption DFT XPS

ABSTRACT

Experimental X-ray photoelectron spectroscopy (XPS) and theoretical density functional theory (DFT) calculations reveal the electronic and structural properties of CoCu catalysts before and after CO adsorption. DFT calculations show that, prior to CO adsorption, CoCu has a high tendency to self-assemble into a Co@Cu core-shell structure, which is in accordance with previous atom probe tomography (APT) results for CoCu-based systems and the known mutually low miscibility of Co and Cu. We demonstrate that Co and Cu are *electronically* immiscible using a density of states (DOS) analysis wherein neither metal's electronic structure is greatly perturbed by the other in "mixed" CoCu. However, CO adsorption on Co is in fact weakened in CoCu compared to CO adsorption on pure Co despite being electronically unchanged in the alloy. Differential charge density analysis suggests that this is likely due to a lower electron density made available to Co by Cu. CO adsorption at coverages up to 1.00 ML are then investigated on a Cu/Co(0001) model slab to demonstrate CO-induced segregation effects in CoCu. Accordingly, a large driving force for a Co surface enrichment is found. At high coverages, CO can completely invert the layer sequence of Co and Cu. This result is echoed by XPS evidence, which shows that the surface Co/Cu ratio of CoCu is much larger in the presence of CO than in H₂.

© 2015 Elsevier B.V. All rights reserved.

1. Introduction

Industrial research with syngas (CO/H₂) at the *Institut Français du Pétrole* (IFP) in the 1970s [1–3] resulted in the formation of shortchain alcohols (up to C_6). A number of catalyst formulations were developed on the basis of CoCu and others. The incentive for choosing these two materials was to design a modified methanol catalyst based on Cu by taking advantage of the chain lengthening properties of Co metal. The authors claimed that the homogeneity of catalyst precursors during the preparation is essential for the final catalyst performance. A modification of the metallic cobalt by alloying was also envisaged even though both metals show low solubility with respect to each other (9% at the most according to the thermodynamic phase diagrams [4]).

Recent studies in our group demonstrated ternary CoCuMn catalysts, prepared by oxalate co-precipitation, to exhibit core@shell structured nanoparticles [5]. In studies with atom probe tomography (APT), Co atoms were shown to form the core in these nanoparticles while all three elements were present in an otherwise Cu dominated shell. Assuming a similar Co@Cu core-shell structure applies to binary CoCu catalysts, pronounced reconstruction was observed in combined TEM/XPS studies (transmission electron microscopy/X-ray photoelectron spectroscopy). The surface composition of such catalyst was found to be strongly dependent on the activation procedure and the composition

of the activating gas [6]. From a theoretical point of view, Ruban et al. and later Nilekar et al. produced density functional theory (DFT) evidence that Cu atom impurities in a cobalt host have a moderate-to-high segregation energy potential [7,8]. This finding is in agreement with thermodynamic predictions; so Cu atoms would be expected to segregate away from Co in a CoCu catalyst.

The oxalate route to mixed-metal catalysts allows core@shell structured CoCu particles to self-assemble by stripping CO₂ molecules off the common oxalate framework [5,6]. On the other hand, inverse Cu@ Co structured particles can be produced on purpose using suitable experimental techniques [9,10]. The Somorjai group has recently studied such catalysts in detail [9,10]. While XPS data under vacuum conditions clearly indicated a Cu@Co core-shell structure, treatment under oxygen made Cu to segregate to the surface. This oxygen-induced segregation was shown to be irreversible: upon reexposure to H₂, the Cu remained on the surface rather than returning subsurface. The Somorjai group argued based on relative oxide formation energies that since CuO is less favorably formed over that of CoO then the driving force to create an oxide in the presence of O₂ could not account for the driving force to segregate Cu to the surface. Instead, they posited that kinetics or strain effects would have to be responsible for Cu segregation and that the permanency of its segregation is due to Cu's lower surface free energy, which itself stems from a lower bulk cohesive energy as compared to Co. Most recent work by the Somorjai group showed some Cu resegregation was in fact possible upon reexposure to H₂, but more Cu remained at the surface than was initially present in as-prepared inverse Cu@Co [9,10].

^{*} Corresponding author. Tel.: +1 509 335 6601; fax: +1 509 335 4806. E-mail address: norbert.kruse@wsu.edu (N. Kruse).

Co/Cu-based catalysts have also recently received attention from the experimental groups of Spivey and Salmeron [11–13]. The structure of on-purpose $Cu@Co_3O_4$ catalysts was elaborated upon by Subramanian et al., who, similar to the Somorjai group, showed that the Cu:Co surface ratio increased 5 times after high temperature oxidation [12]. Carenco et al. later showed that syngas exposure – but not H_2 or CO by themselves – actually depletes Cu@Co core-shell nanoparticles of Co, leading to hollow Cu-rich nanoparticles [13]. Both of these studies illustrate that the Cu@Co core-shell structure is very sensitive to adsorbates and thermal pretreatment, but why this is the case and the degree to which this can be expected is still unknown, and theoretical insights are necessary to further our understanding of CoCu-based catalysts.

Theoretical studies on bimetallic CoCu beyond the single atom Cu impurity work in a Co(0001) host [7,8] are sparse. Most recent investigations of CoCu [14] assumed a CoCu structure with no justification for how the cobalt came to be on the surface, or, equivalently, how it came to be subsurface. To remedy this state of affairs, the present paper uses both experimental techniques and theoretical DFT calculations to elucidate the CoCu segregation behavior. This is done experimentally by examining CoCu-oxalate decomposed in H₂ and CO via XPS, and theoretically by examining the adsorption of a monolayer of Cu on a Co(0001) surface via DFT. We first provide experimental XPS evidence of Co segregation to the surface upon CO adsorption. Our theoretical analysis shows that Cu has a large thermodynamic tendency to segregate to the surface of Cu/Co(0001) leading to Cu surface termination in the absence of CO. Further theoretical analyses reveals how the surface termination of Cu/Co(0001) ultimately alters the adsorption strength of CO compared to pure Co(0001). We follow this with a clear, theoretically explored demonstration of the reversal of Cu/ Co(0001) surface termination by CO adsorption via DFT calculations, which are used to elucidate the experimental results. This CO-induced reversal ultimately results in the inversion of the layer sequence of the CoCu bimetallic system. We conclude with a discussion of the implications of these results with regard to CO hydrogenation using bimetallic CoCu-based catalysts and an outlook to future work.

2. Methodology

2.1. Experimental

CoCu samples were prepared using the oxalate route of coprecipitation. Details of the preparation method were provided earlier [5]. Catalysts with a Co/Cu ratio of 2/1 and 3/1 were selected for characterization by X-ray photoelectron spectroscopy (XPS), CoCu mixed oxalate samples were activated by heating in situ to 400 °C under atmospheric pressure in a flow of 30 mL min⁻¹ of either hydrogen or carbon monoxide in a high-pressure reactor (base pressure 2×10^{-10} mbar) attached to the analytical XPS chamber via a fast sample transfer system. Samples were first pelletized and attached to a sample holder so as to allow resistive heating and temperature control with a thermal couple. Samples could be placed at choice in the reaction chamber or analytical system using a transfer rod and a rotary distribution chamber. Samples were heated resistively while exposing them to hydrogen and carbon monoxide. Samples were transferred into the analysis chamber (residual pressure 5×10^{-11} mbar) after cooling to room temperature and pumping off the gases. Details of the setup were communicated earlier [15]. The X-ray source was operated with an acceleration voltage of 13 kV and an emission current of 10 mA. Non-monochromatized Mg $\mbox{K}\alpha$ and Al K α radiation were used for the analyses. High-resolution scans were made for Co 2p, Cu 2p, C 1s, O 1s, and Cu LMM employing a pass energy of 50 eV with a dwell time of 0.1 s and a step size of 0.05 eV. After subtraction of the Shirley-type background, the core-level spectra were decomposed into components with mixed Gaussian-Lorentzian (G/L) lines using a non-linear least-squares curve-fitting procedure. The C 1s peak at 284.4 eV was used as reference energy for charge correction.

2.2. Theoretical

2.2.1. Computational details

Ab initio density functional theory (DFT) calculations with periodic boundary conditions were performed using the Vienna ab initio simulation package (VASP) [16]. To accurately account for magnetic contributions, any systems containing Co were spin polarized, leaving Cu(111) the only system left in the closed shell approximation. The Perdew–Burke–Enzerhof (PBE) generalized gradient approximation (GGA) [17] was used to describe the electron exchange and correlation functionals with core electrons accounted for by using projector augmented wave (PAW) pseudopotentials [18] to solve the Kohn–Sham equations [19]. The Brillouin zone was sampled using a $5 \times 5 \times 1$ Monkhorst–Pack k–point mesh, and plane waves were expanded to an energy cutoff of 400 eV. We used an electronic energy difference of 1.0×10^{-4} eV and force tolerance of 3.0×10^{-2} eV/Å to establish self consistent field (SCF) and geometric optimization convergence criteria.

With the one exception of pure Cu, all systems in this study were hcp(0001) facets modeled using a four layer $p(2 \times 2)$ supercell with a ~15 Å vacuum layer. If the model catalyst was pure Cu, then a four layer $p(2 \times 2)$ fcc(111) facet with a ~15 Å vacuum layer was used instead. In all models, the bottom two layers were fixed in their bulk positions (with optimized lattice constants of 2.498 Å and 3.639 Å for Co and Cu, respectively) while the top two layers and any adsorbates, if present, were allowed to relax in all directions.

We calculated the adsorption energy according to:

$$E_{\rm ads} = \frac{E^{\rm adsorbates + surface} - E^{\rm surface} - N_{\rm CO} E^{\rm adsorbate}}{N_{\rm CO}}$$
(1)

for CO on Cu(111) and Co(0001) and compared the results with those where the Brillouin zone was sampled using a $6\times6\times1$ Monkhorst–Pack k-point mesh and the energy cutoff was increased to 450 eV. As can be seen from Table 1, the adsorption energies varied by only 0.05 eV at most.

Several previous studies have examined the adsorption of CO on Cu(111) and Co(0001) and as can be seen from Table 1, we get an agreement to within 0.05 eV when comparing our values with those obtained when using a similar computational setup to that of Gajdoš et al. [20]. Recently, the adsorption energies for these systems were also provided

Table 1Comparison of DFT calculated adsorption energies with those reported in the literature. The Gajdoš et al. [20] DFT reference energies were calculated in VASP – as are those calculated here – and the Wellendorff et al. [21] DFT reference energies were calculated in Quantum ESPRESSO. For future reference in this paper, the CO adsorption energies on Cu and Co in perfectly segregated Cu/Co(0001) and 0.25 ML surface Co enriched Cu/Co(0001), respectively, are also shown.

Site	System/setup	PW-91	PBE	Ref. (PW-91) ^a	Ref. (PBE)b
top	CO/Co(0001)	−1.73 eV	-1.68 eV	— 1.65 eV	- 1.53 eV
	400 eV, $(5 \times 5 \times 1)$				
top	CO/Co(0001)	−1.70 eV	−1.65 eV	− 1.65 eV	− 1.53 eV
	450 eV, $(6 \times 6 \times 1)$				
fcc	CO/Cu(111)	−0.88 eV	−0.87 eV		− 0.76 eV
	400 eV, $(5 \times 5 \times 1)$			(top site)	(top site)
fcc	, , , ,	−0.92 eV	−0.91 eV	−0.75 eV	− 0.76 eV
	450 eV, $(6 \times 6 \times 1)$			(top site)	(top site)
top	CO/Cu(111)	− 0.73 eV	−0.72 eV	−0.75 eV	−0.76 eV
	400 eV, $(5 \times 5 \times 1)$			(top site)	(top site)
top	CO/Cu(111)	−0.78 eV	− 0.76 eV		−0.76 eV
	450 eV, $(6 \times 6 \times 1)$			(top site)	(top site)
Cu-fcc	,,,	−0.87 eV	−0.84 eV	-	
	Fully Segregated				
	400 eV, $(5 \times 5 \times 1)$				
Co-top	,	−1.31 eV	−1.26 eV	-	_
	0.25 ML Surface Co				
	400 eV, $(5 \times 5 \times 1)$				

^a Gajdoš et al. [20].

^b Wellendorff et al. [21].

by Wellendorff et al. [21] which show that DFT functionals provide calculated adsorption energies that are in error when compared against experimental values. Some of these errors are significant, but the PBE functional used in this study is one of the most accurate functionals. As a point of reference, our DFT calculated CO adsorption energies on pure Cu(111) and Co(0001) are also compared in Table 1 to the DFT calculated adsorption energies used in the Wellendorf et al. PBE calculations.

For the Cu/Co(0001) systems in Table 1, the adsorption energy was calculated according to

$$E_{\rm ads} = \frac{E^{\rm total}(x,y) - E^{\rm total}(x=0,0) - N_{\rm CO}E_{\rm CO}}{N_{\rm CO}} \eqno(2)$$

where $E^{\text{total}}(x, y)$ is the total DFT energy per supercell of a surface that has x ML equivalents of Co terminating the surface (henceforth, "x ML Co enrichment") and y ML CO coverage. Further, N_{CO} is the number of CO molecules per unit cell and E_{CO} is the total DFT energy of a gas phase CO molecule.

To model Cu/Co(0001) systems, 4 of the top 8 atoms that make up the top two layers of a pure Co(0001) system were replaced with Cu. During permutations of the surface atoms, the Cu atoms were constrained to these top two layers; preliminary calculations showed no significant change in energy if Cu were placed in the third layer as opposed to the second. We note here that since the bottom two layers are meant to electronically represent the semi-infinite Co bulk, the resulting Cu/Co ratio of 1/3 is not reflective of any particular Cu/Co ratio used in experiments.

Cu/Co(0001) atoms were permuted in every way possible so as to guarantee that all unique configurations of Cu and Co in the top two layers of the $p(2\times 2)$ supercell were included in our calculations. This method ensured that the reported energy configurations correspond to minima.

2.2.2. Segregation energy

Segregation energies ($E_{\rm seg}(x,y)$) were defined similarly to Ma and Balbuena, [22] but always in reference to the total energy of the completely segregated Cu/Co(0001) surface having the same adsorbate (CO in this paper) coverage as the (anti)segregated surface. This can be written as

$$E_{\text{seg}}(x,y) = \frac{E^{\text{total}}(x,y) - E^{\text{total}}(x=0,y)}{N_{\text{Co}}}$$
(3)

where $E^{\rm total}(x,y)$ is the same as defined previously, and $N_{\rm Co}$ is the number of Co atoms per supercell brought to the surface layer, which is equivalent to the number of CoCu "swaps" made per supercell. A negative $E_{\rm seg}$ implies that anti-segregating Cu (or equivalently, creating a surface alloy) is energetically favorable, while a positive $E_{\rm seg}$ implies that Cu segregation is more favorable. By comparing each system to an adsorbate coverage-equivalent surface (y) the energy lowering effect of adsorption is removed from the value and only segregation effects are left. As such, we interpret these segregation energies as effective driving forces for (anti)segregation.

2.2.3. Surface energy change

We calculate the surface energy for the case of CO on CoCu as

$$\gamma(x,y) = \frac{E^{\text{total}}(x,y) - N_{\text{Cu}}E^{\text{Cu}}_{\text{bulk}} - N_{\text{Co}}E^{\text{Co}}_{\text{bulk}} - N_{\text{CO}}E_{\text{CO}}}{A_{Cu/Co(0001)}}$$
(4)

where $E^{\rm total}(x,y)$ is as defined above, $E^{\rm Cu}_{\rm bulk}$ and $E^{\rm Co}_{\rm bulk}$ are the total energy of the pure bulk Cu and Co, respectively, and $E_{\rm CO}$ is again the gas phase energy of a single CO. $N_{\rm Cu}$, $N_{\rm Co}$, and $N_{\rm CO}$ are the number of Cu atoms, Co atoms, and CO molecules present per supercell, respectively, while $A_{\rm Cu/Co(0001)}$ is the surface area of a single exposed surface in the

supercell This definition combines the contributions at 0 K from surface creation and CO adsorption, as described by Getman et al. [23], into a single total surface energy. Since the slab used is asymmetric, this definition is also consistent with the surface energy as defined by Reuter et al. [24].

We concern ourselves here only with the *change* in surface energy per CO as compared to the clean, perfectly segregated Cu/Co(0001) system and effectively subtract off the bulk terms:

$$\Delta \gamma(x,y) = \frac{\gamma(x,y) - \gamma(0,0)}{N_{CO}} = \frac{E_y^x - E_0^0 - N_{CO}E_{CO}}{AN_{CO}}$$
 (5)

Division by $N_{\rm CO}$ in Eq. (5) ensures that systems with different surface coverages can be fairly compared. $N_{\rm CO}$ is omitted if no CO is present. We also change to a shorthand notation for surface and total energies of systems with x ML Co enrichment and y ML CO coverage. A negative value of $\Delta \gamma$ is associated with a lowering of surface energy and thus an increase in thermodynamic stability.

3. Results

3.1. XPS surface analysis

We start by determining the relative Co/Cu surface amounts of samples prepared by oxalate co-precipitation. The considerations will be limited to samples with 2/1 and 3/1 nominal Co/Cu ratios. The XPS analysis was performed after in situ decomposition of the oxalate precursors under hydrogen (H₂) or carbon monoxide (CO) at 400 °C. Since we aim at determining the relative Co/Cu surface amounts, we shall focus on an analysis of the Cu 2p and Co 2p spectra. According to Fig. 1, the Cu 2p profiles for samples heated in either H₂ or CO are dominated by the metallic Cu⁰ state (only minor amounts of Cu²⁺ appear on the high binding energy side). More specifically, the spectra are characterized by a doublet spin split of 19.8 \pm 0.1 eV typical of metallic copper. Note that the main peak (932.3 \pm 0.06 eV) is assigned to either Cu⁰ or Cu⁺. This is because both states have statistically similar binding energies, and therefore, the Auger LMM spectra of copper have been used in a qualitative manner to differentiate between the two. As shown elsewhere [6], these Auger spectra demonstrate all samples to contain Cu in the metallic state, including the one treated in the presence of CO, which also shows the presence of some oxidized Cu. As for Co₂Cu₁[CO], a negative binding energy shift is observed for Cu^+ , with $Cu 2p_{3/2}$ and Cu $2p_{1/2}$ binding energies located at 930.7 eV and 950.6 eV, respectively. This anomalous negative binding energy shift has been attributed to tetrahedral Cu⁺ species in cubic spinel oxides [25].

The presence of both $\mathrm{Co^{2+}}$ and $\mathrm{Co^{3+}}$ in the corresponding $\mathrm{Co}\ 2p$ spectra confirms the possible presence of $\mathrm{Co_3O_4}$ spinel phase, at least at the surface. All of the $\mathrm{Co}\ 2p$ spectra contain $\mathrm{Co^0}$, $\mathrm{Co^{2+}}$, and $\mathrm{Co^{3+}}$; however, the relative intensities are varying. It is clear that in the deconvolution of the $\mathrm{Co}\ 2p_{1/2}$, $2p_{3/2}$ excitations is rather involved due to the occurrence of satellite structures. While $\mathrm{Co^0}$ dominates the surface of $\mathrm{Co_2Cu_1[H_2]}$, it is the $\mathrm{Co^{2+}}$ species which dominates both COtreated samples. As discussed elsewhere (by including an analysis of the C 1s and O 1s spectra) [6], $\mathrm{Co\text{-}carbide}$ formation in the CO-treated samples may be responsible for the occurrence of higher oxidation states of $\mathrm{Co}\ (\mathrm{and}\ \mathrm{Cu})$ metal.

An important observation in relation with our XPS studies addresses the relative surface ratio of Co to Cu. The Co/Cu surface ratios (0.86 and 0.68 for Co_2Cu_1 and Co_3Cu_1) are clearly much lower than the bulk nominal ratios for the two samples. Similar Co/Cu surface ratios were also found for the samples activated under He. This is in qualitative accordance with the occurrence of a Co@Cu core-shell structure. Indeed, it has been shown that a Co-rich core phase is encompassed by a Cu-rich shell phase once the CoCu mixed oxalate has decomposed [5,6]. While the Co/Cu ratio is lowest for activation in H2 (or He), for activation in CO, it increases to values of 1.7 and 4.7 for Co₂Cu and Co₃Cu,

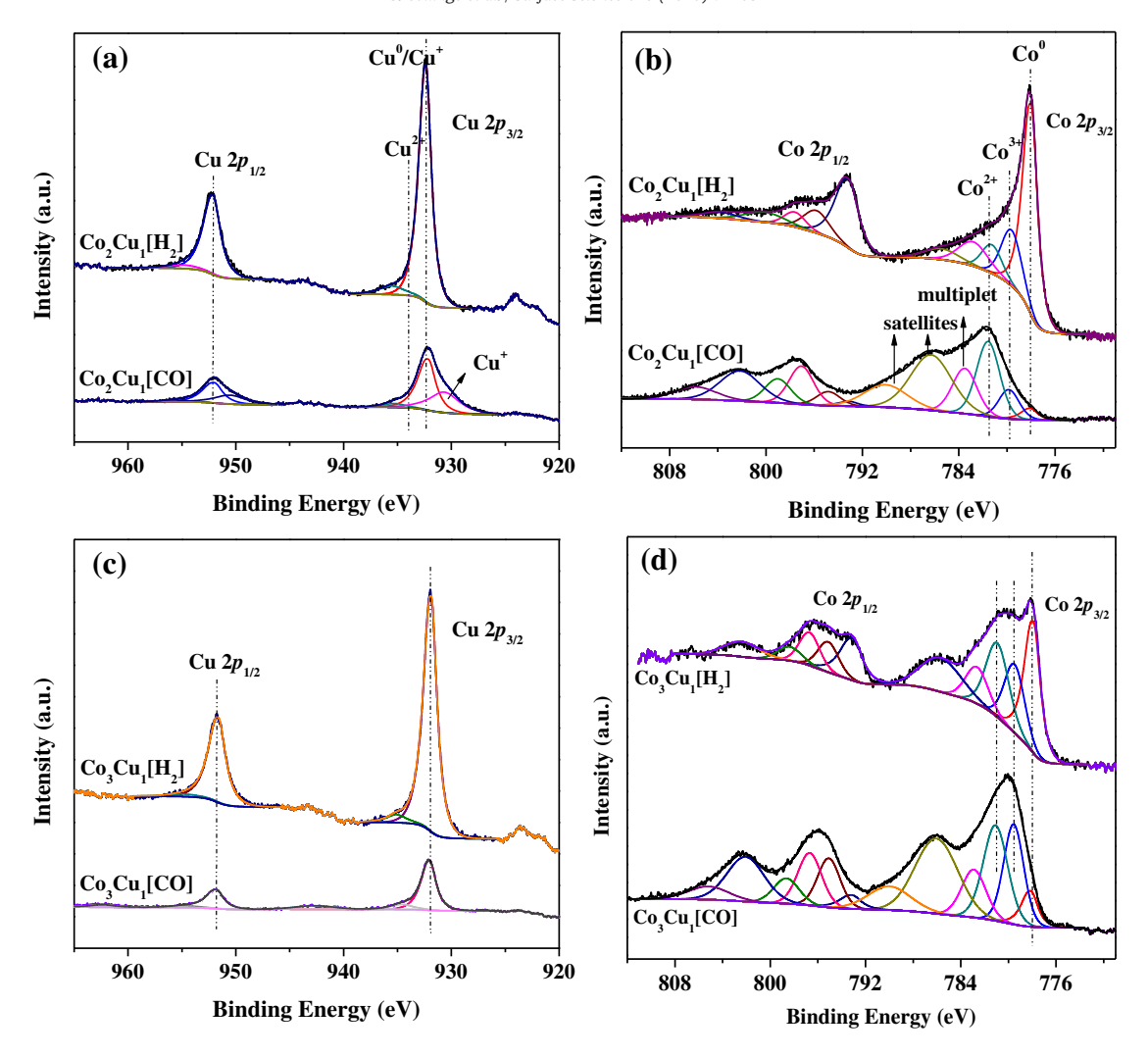


Fig. 1. Cu 2p and Co 2p XPS spectra of CoCu catalysts activated in situ in H₂ and CO gas, respectively. (a and b) Cu and Co 2p spectra for Co₂Cu₁ catalyst; (c and d) Cu and Co 2p spectra for Co₂Cu₁ catalyst.

respectively. Thus, considerable Co segregation takes place under the influence of a CO gas phase. This chemical pumping is intensified because Cu enriched surface phases as present in Co@Cu core-shell structures bind CO relatively weakly. Once the restructuring is consolidated, Co-rich surface phases can decompose adsorbed CO and possibly accumulate surface carbon.

3.2. Clean surface CoCu segregation

Previous atom probe tomography (APT) results have shown that a CoCu-based catalyst self-assembles into a core-shell structure wherein Cu predominates in the shell and Co predominates in the core [5]. To test the hypothesis that this is the result of a large thermodynamic segregation tendency for Cu in Co, the atoms of the top two layers of the model Cu/Co(0001) system were permuted and then segregation energies and surface energy changes were calculated. The resulting premutations create non-equivalent configurations for many of the enrichment levels, examples for which can be found in the SI in Fig. S1. As can be seen in Fig. 2, enriching the surface with Co causes the segregation energy to increase. This indicates that a mixed surface alloy has a very large driving force to segregate completely into a core-shell structure (movement from right to left in Fig. 2(a)). This driving force is largest at 0.50 ML surface Co enrichment but is also large and positive for all surface Co concentrations. Fig. 2(b) shows the corresponding values of $\Delta \gamma$ for the clean surface as the surface is enriched with Co. As can be seen, $\Delta\gamma$ steadily increases as more Co is brought to the surface (and likewise, Cu is pushed subsurface). Thus, any degree of CoCu alloying would always favor perfect segregation. This phenomenon provides a convincing account of the CoCu coreshell structure found in our experimental APT results.

3.3. Electronic properties of CoCu and CO adsorption

The CoCu core-shell structure was further studied through calculations of the projected density of states (pDOS) for Co and Cu in the top and second layers of Co(0001), Cu(111), perfectly segregated Cu/Co(0001), and Cu/Co(0001) at 0.25 ML surface Co enrichment (henceforth " $Cu_{0.75}Co_{0.25}/Co(0001)$ "). The results can be seen in Fig. 3 where the unique energetic behavior of each metal is represented. As usual, the features are dominated by the d-band since the sp-band is too diffuse. To place all systems on equal energetic footing, each system is referenced to its vacuum energy. Fermi levels are indicated with vertical lines.

Comparing the pDOS between the pure metals and the two configurations of the CoCu alloy, the most striking feature of the plots in Fig. 3 is the overall *lack* of change as Co and Cu systems are "alloyed." There is some noticeable change in the shape of each band, indicating rehybridization occurs, but the energetic placement of most of the Cu and Co d-states is the same before and after alloying. The d-states of Co

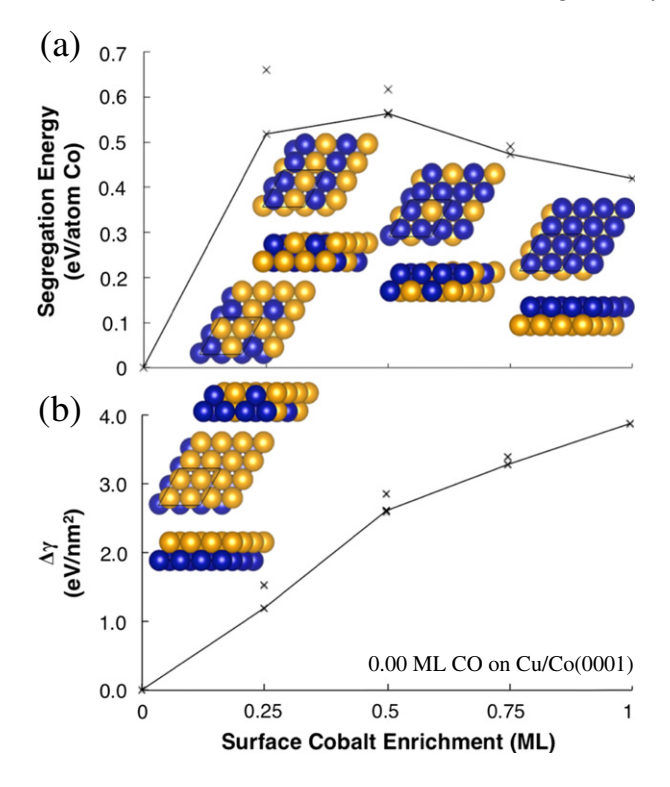


Fig. 2. (a) Segregation energies and (b) surface energy changes for Cu/Co(0001) in the absence of CO. Data points correspond to the different configurations that can be achieved through permutation of the Co and Cu in the top two layers of the surface. The solid lines connect the minimum energy configurations, for which top and side views are shown inset. The orange spheres are Cu atoms and the blue spheres are Co atoms.

change the least, while the Cu d-states show a moderate shift in energy; the surface Cu d-band center moves toward the Fermi level by ~0.6 eV.

In likewise fashion, the Fermi levels of both metals barely move at all in relation to the vacuum energy. The Fermi level of Co moves insignificantly (the shift is ± 0.04 eV), while that of the Cu shifts down by $\sim\!0.3$ eV. From these shifts we can infer that Co is practically unaffected by the presence of Cu, while Cu is slightly activated by Co. However, in no case does the d-band of Cu become partially vacant; the Fermi level is always above the top edge of the d-band. The implication here is that these changes in the electronic structure of Cu are not enough to change Cu's nobility.

These aforementioned energetic changes are represented by d-band centers, ε_d – ε_F , and work functions, Φ , and are shown in Table 2. Based on the previous qualitative analysis and the results presented in this table, we conclude that the Cu and the Co in Cu/Co(0001) are electronically unaffected by their respective alloying. To examine the effect of Cu on Co further, we compare the adsorption energies for CO on a Cu(111) surface, a Co(0001) surface, a Cu/Co(0001) surface, and a Cu_{0.75}Co_{0.25}/ Co(0001) surface, which is given in Table 1. CO adsorption on Cu in the fully segregated Cu/Co(0001) is very similar to CO adsorption in a fcc hollow site of pure Cu(111) (-0.84 eV vs. -0.87 eV), which reflects Cu's persistent nobility even when in contact with Co. In contrast to CO adsorption on Cu, CO adsorption on Co in Cu_{0.75}Co_{0.25}/Co(0001) is markedly different than on Co in Co(0001) (-1.26 eV vs. -1.68 eV). Even though Co in Cu_{0.75}Co_{0.25}/Co(0001) is electronically very similar to Co in pure Co(0001), CO adsorbs on the surface Co in $Cu_{0.75}Co_{0.25}$ Co(0001) much more weakly. In the forgoing analysis, we make the tacit assumption that no surface rearrangement is occurring beyond that explicitly invoked in the model. These results are correlated to the surrounding environment of the Co within the first layer: the surface Co in Cu_{0.75}Co_{0.25}/Co(0001) is surrounded by Cu, while in pure Co(0001), it is surrounded by Co. In particular, the electron density in the surface Cu of Cu/Co(0001) shows less change than the electron

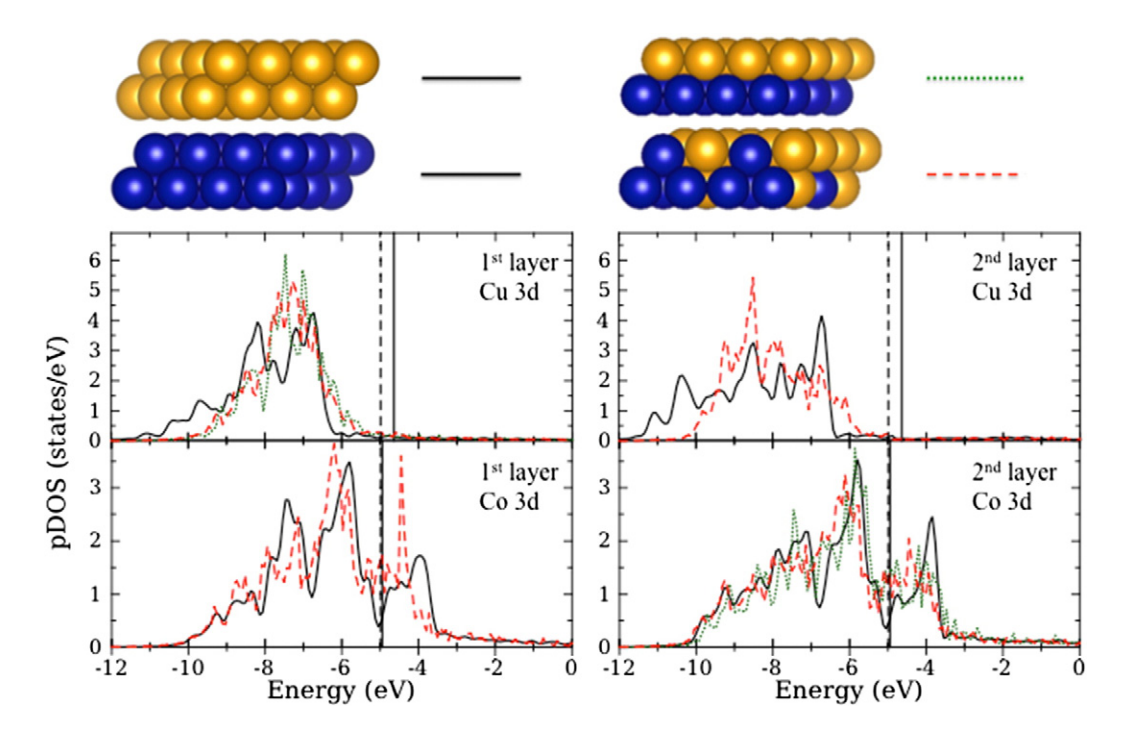


Fig. 3. Projected density of states (pDOS) for Co(0001), Cu(111), Cu/Co(0001), and Cu_{0.75}Co_{0.25}/Co(0001). The energies are referenced with respect to the vacuum energy. Solid black lines correspond to the pure metals, green dotted lines correspond to the perfectly segregated surface, and red dashed lines correspond to Cu_{0.75}Co_{0.25}/Co(0001). Vertical solid and dashed lines indicate the Fermi levels for pure Co(0001) or Cu(111), and both alloyed CoCu systems, respectively. Fermi level shifts were too small to visually distinguish between the perfectly segregated and 0.25 ML surface Co enriched systems and therefore are represented by a single vertical dashed line.

Table 2

Calculated d-band centers (in reference to the metal Fermi level) and work functions, $\epsilon_d - \epsilon_F$ and Φ , respectively, for Co and Cu in Co(0001), Cu(111), Cu/Co(0001), and Cu_{0.75}Co_{0.25}/Co(0001). The table is set up to allow easy comparison between the pure metals and the Cu/Co(0001) surfaces, where deviations from the pure metal values can be viewed as deviation from electronic properties of the pure metal. ϵ_d^{surf} denotes the d-band center of the d-band projected onto a surface atom, while $\epsilon_d^{subsurf}$ is d-band center projected similarly for those atoms in the subsurface (the second layer). The values in this table correspond to the pDOS shown in Fig. 3.

	Φ	$arepsilon_d^{ m surf} - arepsilon_f$	$arepsilon_d^{ m subsurf} - arepsilon_f$
Cu in	4.66 eV	−3.11 eV	−3.60 eV
Cu(111)			
Cu in Cu/Co(0001)	4.90 eV	−2.50 eV	no subsurface Cu
Cu in	4.99 eV	−2.49 eV	−3.05 eV
Cu _{0.75} Co _{0.25} /Co(0001)			
Co in	4.95 eV	−1.99 eV	− 1.99 eV
Co(0001)	400 17		2.07. 1/
Co in Cu/Co(0001)	4.90 eV	no surface Co	−2.07 eV
Co in	4.99 eV	- 1.98 eV	−2.17 eV
Cu _{0.75} Co _{0.25} /Co(0001)			

density of the surface Co of pure Co(0001). We see this in Fig. 4, which shows the differential charge density of CO adsorption in the fcc hollow sites of Cu in Cu(111) and the fully segregated Cu/Co(0001), and in Fig. 5, which shows the differential charge density of CO adsorption on the top sites of Co in Co(0001) and Cu_{0.75}Co_{0.25}/Co(0001). In Fig. 4, the atoms that surround the three Cu atoms involved in CO adsorption show equivalent change in charge density whether the surface is pure Cu(111) (Fig. 4(a)) or fully segregated Cu/Co(0001) (Fig. 4(b)). The differential charge elsewhere is practically equivalent as well. This reflects very well the minor change in CO adsorption energy seen in Table 1. Conversely, the differential charge density for CO adsorption on Co(0001) seen in Fig. 5 shows a distinct loss around the surrounding

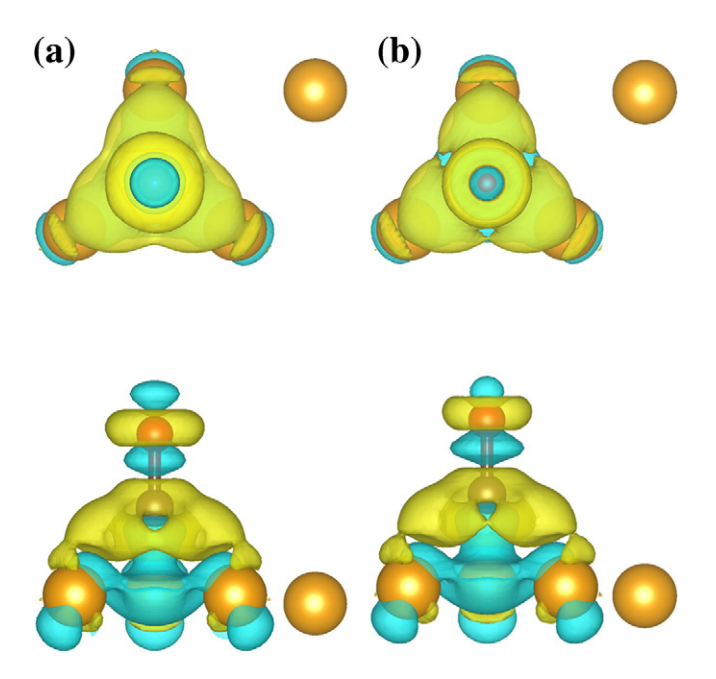


Fig. 4. Top and side views of the differential charge density of CO adsorption on Cu's in (a) Cu(111) and (b) the fully segregated Cu/Co(0001). Blue shading indicates charge loss while yellow shading corresponds to charge gain. The lack of any significant change in the differential charge density between the two systems is posited to be responsible for the similarity of CO adsorption strength between the two systems. The color legend for the spheres is the same as Fig. 1, except the red spheres are the oxygen atoms and the brown spheres are the carbon atoms. The isosurface level is set at 0.003 electrons/Bohr³.

Co atoms (Fig. 5(b)), which is not present around the surrounding Cu atoms in the $\text{Cu}_{0.75}\text{Co}_{0.25}/\text{Co}(0001)$ system (Fig. 5(a)). The only region of charge density gain is around the CO adsorption site for the partially segregated $\text{Cu}_{0.75}\text{Co}_{0.25}/\text{Co}(0001)$ system. We therefore posit that the Cu in $\text{Cu}_{0.75}\text{Co}_{0.25}/\text{Co}(0001)$ cannot similarly contribute to the chemisorption of CO and that this might account for the lowering of the CO adsorption energy seen in Table 1.

To study this further, we also examined the differential charge density of the clean metal surfaces of Co(0001) and Cu_{0.75}Co_{0.25}/Co(0001), in which each surface Co is completely surrounded at the surface by either Co or Cu as shown in Fig. 6. The metal atoms in Fig. 6 are kept in the same position as those of the CO adsorption systems in Fig. 5 and then the surface Co atom – which is eventually the Co adsorbent atom – is removed to create a vacancy in the surface. The charge densities of these defective systems ($\rho_{\rm surface\ with\ vacancy}$) and that of the lone Co atom ($\rho_{\rm Co\ atom}$) that is removed are then calculated and compared to the charge densities of the metals without the vacancy ($\rho_{\rm full\ surface}$), which are the systems in Fig. 4 in which the CO has been removed. The forgoing explanation can be written in equation form as

$$\Delta \rho = \rho_{\text{full surface}} - \rho_{\text{surface with vacancy}} - \rho_{\text{Co atom}}$$

This differential charge density qualitatively shows the amount of charge that is being shared with the surface Co atom by the surrounding atoms. Thus, in effect, Fig. 6 shows the extent to which the metal atoms surrounding the surface Co atom are able to provide/remove charge to/ from the surface Co atom. What we see in Fig. 6 is a much smaller amount of charge transfer between the surface Co atom and its surrounding surface Cu atoms (Fig. 6(b)) than between the surface Co atom and its surrounding surface Co atoms (Fig. 6(a)). This shows that Cu makes its electrons much less available to the surface Co atom than does other Co. This is further highlighted when looking at the interactions between the first and the second layer in the Cu_{0.75}Co_{0.25}/ Co(0001) system shown in Fig. 6(b): there is larger amount of charge transfer between the Co atom in the first layer and the Co atoms in the second layer as compared to the corresponding charge transfer between the Co atom in the first layer and the surrounding Cu atoms in the first layer. Therefore, even before CO adsorbs onto these systems, there is already a discrepancy between the amount of charge made available by pure Co(0001) and the amount of charge made available by $Cu_{0.75}Co_{0.25}/Co(0001)$. Such observations help explain the 0.42 eV drop in adsorption energy when the adsorbent Co is surrounded by Cu instead of other Co. Therefore, we speculate that the adsorption energy would be further lowered by the presence of even more adjacent Cu and would expect to see a similar dependence on systems containing noble metals due to their propensity to remain close shelled.

3.4. CO-induced Co antisegregation

X-ray photoelectron spectroscopy (XPS) experiments with CoCu catalysts have demonstrated a CO-induced increase in their surface Co/Cu ratios. This is strongly indicative of a surface restructuring during which Co is chemically "pumped" to the surface. To further support this experimental evidence the Cu/Co(0001) model surface was again subjected to surface permutations, but this time at various CO coverages. The $p(2 \times 2)$ supercell allows for four CO coverages: 0.25 ML, 0.50 ML, 0.75 ML, and 1.00 ML. With each degree of coverage present, the surface was permuted once more, similarly to those performed for the clean catalyst. However, with CO adsorbed on the surface, much of the degeneracy present for a clean catalyst is removed, and many more Cu/Co(0001) configurations exist (for an example of non-equivalent configurations at the same CO coverage and Co enrichment level, see Fig. S2 in the SI). The segregation and surface energies for each configuration were calculated and the results are presented in Fig. 7. Minimum energy configurations are shown as insets for each CO coverage.

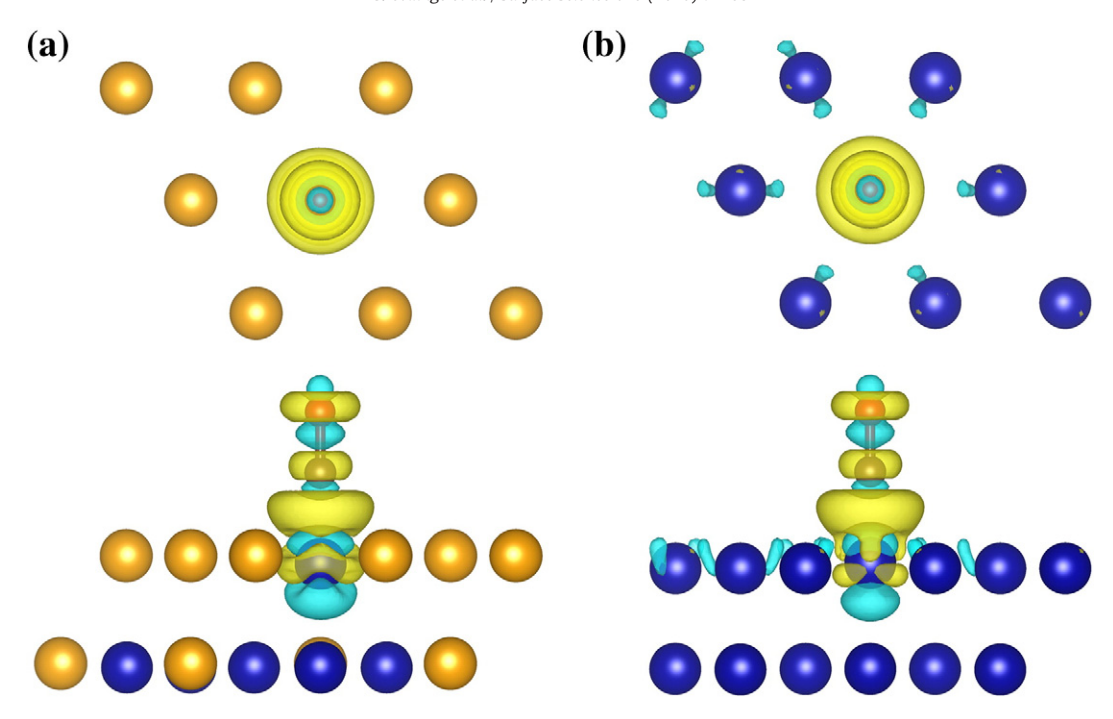


Fig. 5. Top and side views of the differential charge density for CO adsorption on Co in (a) $Cu_{0.75}Co_{0.25}/Co(0001)$, in which the surface Co adsorbent atom is surrounded by Cu, and (b) the pure Co(0001) system, where the adsorbent atom is surrounded by Co in the first layer. The charge density loss evident on the surrounding Co in the pure Co(0001) system that is not present in the Cu/Co(0001) system is posited to be the source of the higher adsorption energy of CO on Co in pure Co(0001) over that on Co in Cu/Co(0001). The isosurface level is set at 0.003 electrons/Bohr³.

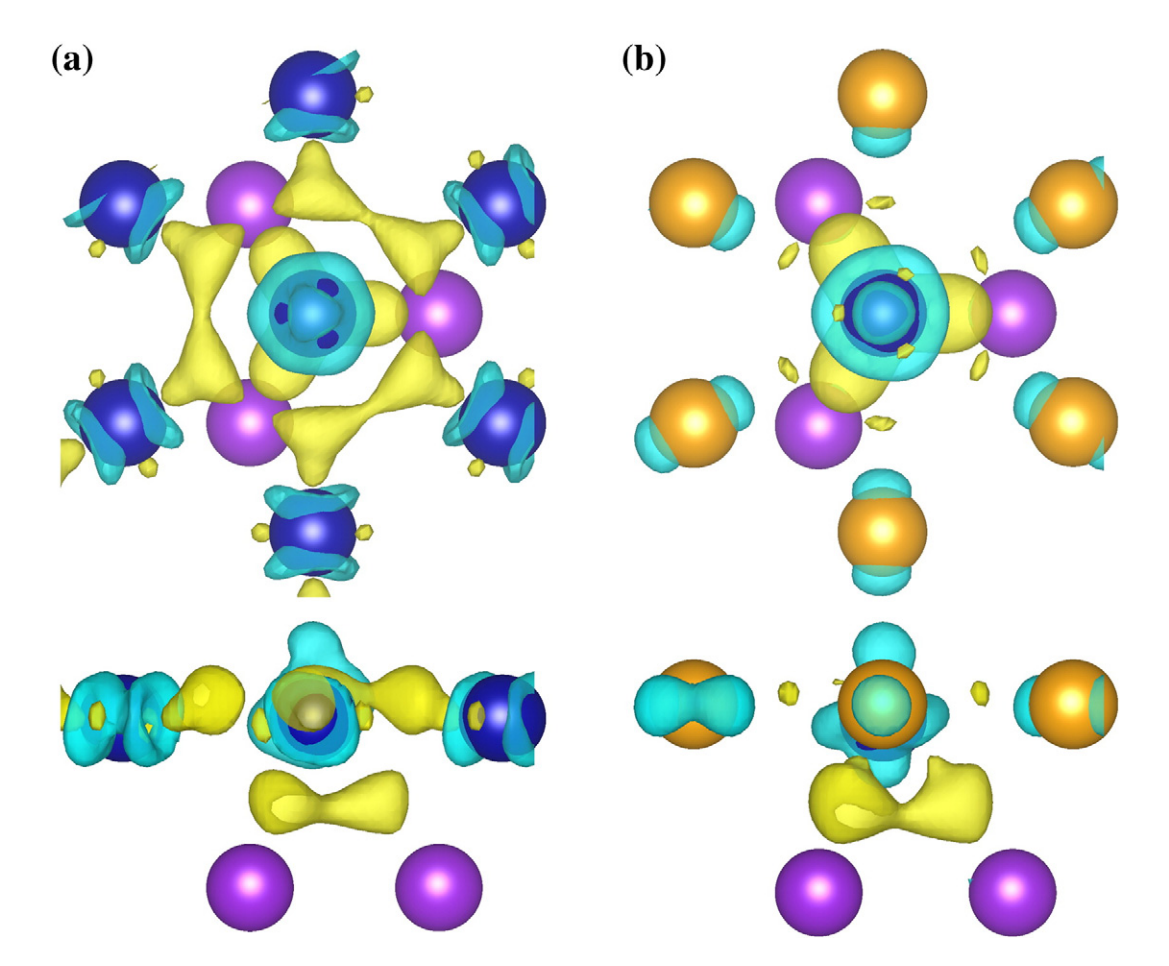


Fig. 6. Top and side views of the differential charge density of Co adsorbent atoms in (a) the pure Co(0001) system and (b) the $Cu_{0.75}Co_{0.25}/Co(0001)$ system. The blue and yellow shaded regions represent charge loss and charge gain, respectively. There is clearly more charge transfer between surface metal atoms in the Co(0001) system than in the Co(0001) system. This is posited to contribute to the -0.4 eV discrepancy in CO adsorption energy between the two systems. The Co atoms in the top layer are blue spheres, the Co atoms in the second layer are purple spheres, and the Cu atoms are orange spheres. The isosurface level is set at 0.007 electrons/Bohr³.

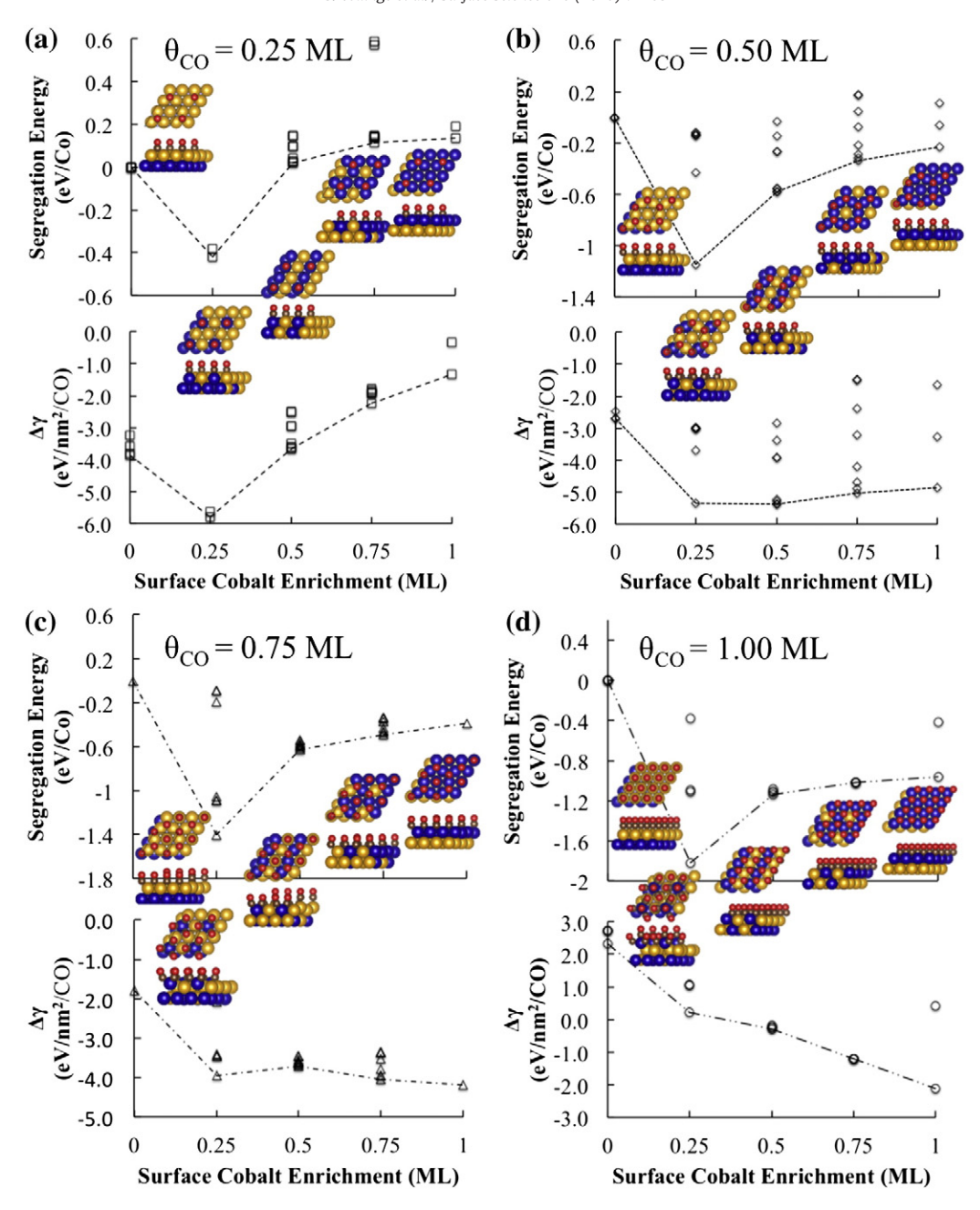


Fig. 7. Segregation energies and surface energy changes for CO adsorbed on Cu/Co(0001) at (a) 0.25 ML CO, (b) 0.50 ML CO, (c) 0.75 ML CO, and (d) 1 ML monolayer of CO. For each CO coverage and Co enrichment, there are many possible configurations, which are represented by data points in each plot. Lines connect the minimum energy configurations for each CO coverage/Co enrichment system and their corresponding structures are shown as insets. Each abscissa range is set so as to best show the effect of enriching the surface with Co for that coverage and as such does not give a direct impression of the differences between coverages. These graphs are combined in Fig. 4 to provide a full comparison of Co enrichment at each degree of CO coverage. The color legend for the spheres is the same as in Fig. 3.

An evident feature of these graphs concerns the segregation energies. A precipitous drop in segregation energy is associated with the first increase in surface Co concentration. This means that any amount of adsorbed CO strongly induces Co pumping where adsorbing CO provides a large driving force to reverse the segregation tendency of the clean CoCu surface.

As can be seen in Fig. 7(a), at 0.25 ML CO coverage, this initial drop ($-0.42\,$ eV/Co), which is associated with 0.25 ML surface Co enrichment, is the only negative value of segregation energy; increasing surface Co concentration beyond this would require an input of energy. $\Delta\gamma$ mirrors this result, and in this case the value of $\Delta\gamma$ increases steadily as surface Co is enriched beyond 0.25 ML. At low CO coverages, only low surface Co concentrations are thermodynamically favorable.

At 0.50 ML CO coverage – Fig. 7(b) – there is a similar large drop (-1.15 eV/Co) in segregation energy upon surface Co enrichment to 0.25 ML, but further enriching the surface with Co does not result in positive segregation energies like in the 0.25 ML CO coverage case. However, although Co concentrations past 0.25 ML have negative segregation energies, the values of $\Delta\gamma$ reveal that 0.25 ML and 0.50 ML surface Co enrichment is overall more thermodynamically favorable than higher surface Co concentrations. Therefore, we conclude that once again only low surface Co concentrations are attainable.

A 0.75 ML CO coverage results in a similar segregation energy behavior as the 0.50 ML CO coverage, but the behavior of $\Delta\gamma$ is quite different as surface Co enrichment is increased. We again have a large decrease (-1.40 eV/Co) in segregation energy at 0.25 ML surface

Co enrichment, which is followed by much smaller, yet negative, segregation energies. Conversely, the plot of $\Delta\gamma$ shows a local minimum at 0.25 ML Co enrichment, but an absolute minimum at 1.00 ML Co enrichment. Thus, the presence of a 0.75 ML CO coverage on Cu/Co(0001) will ultimately result in a complete <code>inversion</code> of the CoCu layer sequence; the topmost layer of the catalyst can become 1.00 ML enriched with surface Co.

The largest driving force (-1.82 eV/Co) is obtained at 1.00 ML CO coverage enriching the surface to 0.25 ML Co. However, by looking at the value of $\Delta\gamma$ for this system, we can see that this is mostly due to the fact that a monolayer of adsorbed CO on a completely segregated Cu/Co(0001) surface is unstable (positive $\Delta\gamma$ of +2.35 eV/nm²/CO), and not due to any particularly high stability of the resulting Cu_{0.75}Co_{0.25}/Co(0001) system, which actually has a positive $\Delta\gamma$ value of 0.11 eV/nm²/CO. Even still, this full monolayer of CO does become more and more stable as Co is brought to the surface, and this progression results in a minimum energy configuration at 1.00 ML Co enrichment. This is something of a moot point, however, since 0.75 ML CO coverage is enough to induce the inversion of Cu and Co layers and since the values of $\Delta\gamma$ at 1.00 ML CO coverage are never lower than the values of $\Delta\gamma$ at 0.75 ML CO coverage regardless of the surface enrichment of Co, as can be seen by examining Fig. 8.

By plotting all the segregation energies and $\Delta\gamma$ data presented so far in Fig. 8, we can see that segregation energies are highest for the clean surface and lowest for the 1.00 ML CO coverage system with a monotonic change as the CO coverage increases or decreases (movement along

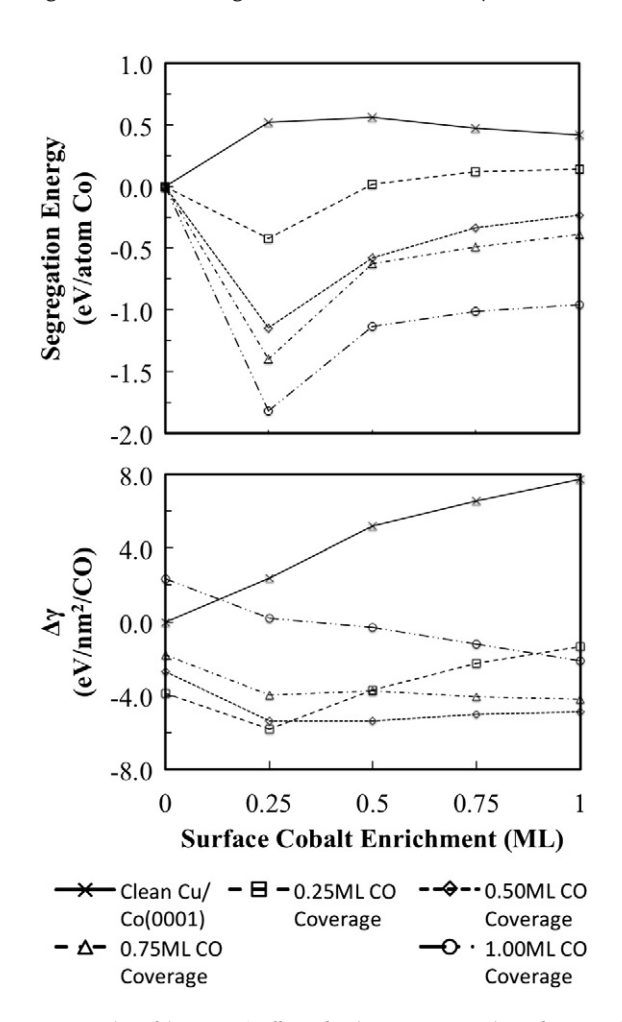


Fig. 8. Summary plots of the energetic effects of each CO coverage on the surface Co enrichment of Cu/Co(0001). The data points and lines used are consistent with those presented in Figs. 2 and 7. It should be noted that for the clean surface, $\Delta \gamma$ has units of eV/nm² and not eV/nm²/CO.

the y-axis instead of the x-axis). That is, with increasing CO coverage, the driving force for segregation of Co and Cu is gradually altered from favoring a Cu terminated surface to a Co terminated one.

Conversely, there is no monotonicity in the plot of $\Delta\gamma$ as the CO coverage is increased up to 1.00 ML. In order to fully understand the implications of this plot, we must break down the trends for each CO coverage, and in this vain, we make the following observations:

- The lowest value of $\Delta \gamma$, and thus the most favorable configuration overall, is achieved at a 0.25 ML surface Co enrichment and a CO coverage of 0.25 ML. Thus, at even low CO coverages Co enrichment at the surface is thermodynamically favorable.
- The lowest overall values of $\Delta\gamma$ at the remaining degrees of Co enrichment (0.50 ML–1.00 ML) are all achieved at a CO coverage of 0.50 ML. However, the highest concentrations of surface Co do not correspond to the absolute minimum energy configuration of 0.50 ML CO, which is achieved at 0.50 ML Co enrichment. This is very closely followed in favorability by the configuration at 0.25 ML Co enrichment a mere 0.03 eV/nm²/CO higher than the value of $\Delta\gamma$ at 0.50 ML enrichment, which is well within the error of DFT. The 0.50 ML CO coverage results in a slight increase in likelihood of pumping Co to 0.50 ML surface enrichment. It is also worth noting that the 0.75 ML and 1.00 ML surface Co enriched configurations are a mere 0.36 eV/nm²/CO and 0.53 eV/nm²/CO higher than the 0.50 ML Co enriched configuration.
- The next most favorable configuration at the two highest surface cobalt enrichments is achieved by 0.75 ML of CO, and for this coverage, complete surface Co enrichment is the absolute minimum energy configuration.
- Fig. 8 also confirms what was noted previously, that 1.00 ML CO coverage is always unfavorable compared to lower coverages no matter what amount of Co is pumped to the surface. This is due in part to the large nearest neighbor lateral interaction between the CO molecules, which may play a fundamental role in the underlying Fischer–Tropsch reaction mechanism on such catalysts [26].

4. Conclusion

We have shown here that Co and Cu have a very strong tendency to segregate into a Cu shell atop a Co core and that CO adsorption on this fully segregated surface is essentially very similar to that on pure Cu (provided that no surface rearrangement occurs). On the other hand, CO adsorption on Co in $\text{Co}_{0.25}\text{Cu}_{0.75}/\text{Co}(0001)$ is markedly weaker than that on pure Co even though Co appears to be electronically unaffected by the presence of Cu according to our density of states analysis.

Whilst CoCu appears to exist as a Co@Cu core-shell structure we show that CO adsorption can induce an antisegregation of Cu and Co in CoCu whereby Co is chemically "pumped" to the surface and is effectively exchanged for surface Cu. We illustrate this using an experimental XPS analysis, which shows a significant increase in the Co/Cu surface ratio upon interaction with CO gas, and using further DFT calculations on the various permutations of the Cu/Co(0001) surface. The DFT calculations show that the CO covered anti-segregated surface is thermodynamically favored over that of a CO covered fully segregated surface. If CO is present at high coverages, the surface can become 1.00 ML enriched in Co; the layer sequence of CoCu can become completely inverted.

To put the results of this paper into a more general context, we retain that our combined theoretical–experimental approach clearly demonstrates that major restructuring occurs with segregated Co@ Cu core-shell catalyst particles as used for the CO hydrogenation to higher terminal alcohols. The next step will be to include CO dissociation because we anticipate that surface carbon and oxygen formed during this step are essential in the construction of the catalytically active phase [27]. Based on our density of states results on Co and Cu in Cu/Co(0001) and on the comparison of CO adsorption on pure

Co(0001) and on Cu/Co(0001), we suspect CO dissociation to be site selective. With this in mind, Ge and Neurock have previously established that the activation energies for CO dissociation on pure Co flat surfaces are prohibitively high, and that CO dissociation is only feasible on stepped and kinked Co surfaces [28]. We would therefore not expect to see CO dissociation occurring on flat Cu/Co(0001), though facets with this orientation may well play a role in establishing stable particle morphologies. With this, we further conclude that future work into CO dissociation on CoCu will include stepped and kinked surfaces.

5. Supplementary Information

The Supplementary Information contains two figures, both of which provide example configurations that correspond to equivalent CO coverage and surface Co enrichment. Figure S1 gives examples of two clean Cu/Co(0001) surface configurations that have equivalent surface Co enrichment. Figure S2 gives examples of two 0.25 ML CO adsorbed Cu/Co(0001) surface configurations also with equivalent surface Co enrichment. These figures are meant to clarify the distinction between vertically plotted data points in Figs. 2 and 7.

Acknowledgements

This work was supported by institutional funds provided to J.S.M. and N.K. from the Voiland School of Chemical Engineering and Bioengineering and the National Science Foundation under contract No. CBET-1438227. It was also partially funded by USDA/NIFA through Hatch Project no. WNP00807 titled: "Fundamental and Applied Chemical and Biological Catalysts to Minimize Climate Change, Create a Sustainable Energy Future, and Provide a Safer Food Supply." G.C., Seattle Chapter ARCS Fellow, gratefully acknowledges financial support from the Achievement Rewards for College Scientists foundation.

Appendix A. Supplementary data

Supplementary data to this article can be found online at http://dx. doi.org/10.1016/j.susc.2015.10.014.

References

- [1] A. Sugier, E. Freund, US 4,122,110, (1978).
- [2] B. C. P. Courty, D. Durand, C. Verdon, US 4,780,481, (1988).
- [3] D.D.P. Courty, E. Freund, A. Sugier, J. Mol. Catal. 17 (1982) 241.
- [4] T. Nishizawa, K. Ishida, Bull. Alloy Phase Diagr. 5 (1984) 161.
- [5] Y. Xiang, V. Chitry, P. Liddicoat, P. Felfer, J. Cairney, S. Ringer, N. Kruse, J. Am. Chem. Soc. 135 (2013) 7114.
- [6] Y. Xiang, R. Barbosa, N. Kruse, ACS Catal. 4 (2014) 2792.
- [7] A.U. Nilekar, A.V. Ruban, M. Mavrikakis, Surf. Sci. 603 (2009) 91.
- [8] A.V. Ruban, H.L. Skriver, J.K. Nørskov, Phys. Rev. B 59 (1999) 15990.
- [9] S. Alayoglu, S.K. Beaumont, G. Melaet, A.E. Lindeman, N. Musselwhite, C.J. Brooks, M.A. Marcus, J. Guo, Z. Liu, N. Kruse, G.A. Somorjai, J. Phys. Chem. C 117 (2013) 21803.
- [10] S.K. Beaumont, S. Alayoglu, V.V. Pushkarev, Z. Liu, N. Kruse, G.A. Somorjai, Faraday Discuss. 162 (2013) 31.
- [11] M.L. Smith, N. Kumar, J.J. Spivey, J. Phys. Chem. C 116 (2012) 7931.
- 12] N.D. Subramanian, C.S.S.R. Kumar, K. Watanabe, P. Fischer, R. Tanaka, J.J. Spivey, Catal. Sci. Technol. 2 (2012) 621.
- [13] S. Carenco, A. Tuxen, M. Chintapalli, E. Pach, C. Escudero, T.D. Ewers, P. Jiang, F. Borondics, G. Thornton, A.P. Alivisatos, H. Bluhm, J. Guo, M. Salmeron, J. Phys. Chem. C 117 (2013) 6259.
- [14] X.-C. Xu, J. Su, P. Tian, D. Fu, W. Dai, W. Mao, W.-K. Yuan, J. Xu, Y.-F. Han, J. Phys. Chem. C 119 (2015) 216.
- 15] S.P. Chenakin, R. Prada Silvy, N. Kruse, J. Phys. Chem. B 109 (2005) 14611.
- [16] G. Kresse, J. Hafner, Phys. Rev. B 49 (1994) 14251.
- [17] J.P. Perdew, K. Burke, M. Ernzerhof, Phys. Rev. Lett. 77 (1996) 3865.
- [18] M.C. Payne, M.P. Teter, D.C. Allan, T.A. Arias, J.D. Joannopoulos, Rev. Mod. Phys. 64 (1992) 1045.
- [19] W. Kohn, L.J. Sham, Phys. Rev. 140 (1965) A1133.
- [20] M. Gajdoš, A. Eichler, J. Hafner, J. Phys. Condens. Matter 16 (2004) 1141.
- [21] J. Wellendorff, T.L. Silbaugh, D. Garcia-Pintos, J.K. Norskov, T. Bligaard, F. Studt, C.T. Campbell, Surf. Sci. 640 (2015) 36.
- 22] Y. Ma, P.B. Balbuena, Surf. Sci. 602 (2008) 107.
- [23] R.B. Getman, Y. Xu, W.F. Schneider, J. Phys. Chem. C 112 (2008) 9559.
- [24] K. Reuter, M. Scheffler, Phys. Rev. B 65 (2001) 035406.
- [25] D.A. Kukuruznyak, J.G. Moyer, N.T. Nguyen, E.A. Stern, F.S. Ohuchi, J. Electron. Spectrosc. Relat. Phenom. 150 (2006) 275.
- [26] M. Zhuo, A. Borgna, M. Saeys, J. Catal. 297 (2013) 217.
- [27] J. Schweicher, A. Bundhoo, N. Kruse, J. Am. Chem. Soc. 134 (2012) 16135.
- [28] Q. Ge, M. Neurock, J. Phys. Chem. B 110 (2006) 15368.